A R C H I V E S O F M E T A L L U R G Y A N D M A T E R I A L S
Volume 56 2011 Issue 4
DOI: 10.2478/v10172-011-0114-9

J. KOWALSKI*, J. PSTRUŚ**, S. PAWLAK**, M. KOSTRZEWA***, R. MARTYNOWSKI*, W. WOŁCZYŃSKI**

INFLUENCE OF THE REFORGING DEGREE ON THE ANNIHILATION OF THE SEGREGATION DEFECTS IN THE MASSIVE FORGING INGOTS

WPŁYW STOPNIA PRZEKUCIA NA ZANIK DEFEKTÓW SEGREGACYJNYCH W MASYWNYM WLEWKU KUZIENNYM

The structural zones of the forging ingot have been distinguished. Some segregation defects within these zones have been described. An observation of the defects has been carried out with the use of scanning microscopy and scanning acoustic microscopy. Some defects revealed by the scanning acoustic microscopy have been subjected to the 3D computer visualization. A difference between localization and difference between morphology of carbides precipitated in the columnar structure and equiaxed structure has been shown. A given ingot was subjected to the plastic deformation with different reforging degree. The samples were taken from different segments of the reforged ingot. A density was determined for each ingot segment. A degree of consolidation was determined after ingot reforging. Once again the scanning acoustic microscopy was applied to determine the annihilation of the segregation defects in the forging ingot structure. A new definition of the consolidation factor after the reforging has been proposed.

Keywords: consolidation degree, structural zones, segregation defects

Wyróżniono strefy strukturalne we wlewku kuziennym. Opisano defekty segregacyjne w wyróżnionych obszarach jego struktury. Przeprowadzono obserwacje defektów z użyciem mikroskopu skaningowego oraz ultradźwiękowego. Dokonano trójwymiarowej komputerowej wizualizacji defektów odkrytych mikroskopem ultradźwiękowym. Pokazano różnice w lokalizacji i morfologii węglików wydzielonych w strukturze kolumnowej oraz w strukturze równoosiowej. Wybrany wlewek kuzienny poddano przeróbce plastycznej z różnymi stopniami przekucia. Pobrano próbki materiału z poszczególnych segmentów przekutego wlewka. Oceniono gęstość materiału w badanych segmentach wlewka. Oceniono stopień zagęszczenia materiału w wyniku przekucia. Ponownie użyto mikroskopu ultradźwiękowego aby ocenić zanik defektów segregacyjnych w strukturze wlewka kuziennego. Zaproponowano nową definicję wskaźnika zagęszczenia wlewka po przekuciu.

1. Introduction

An analysis of the segregation defects within some ingots, rolls, and massive or middle-massive casts has a crucial importance particularly when an ingot is subjected to the plastic deformation. Solidification process is to some extent complicated, so that, it leads to the formation of different segregation defects, Fig. 1.

The chilled equiaxed structure is the result of the first contact between the liquid steel and cold mould. The columnar structure appears when the heat is abstracted from the solid / liquid interface into the surrounding air through the mould. The oriented dendrites are also the product of unidirectional solidification but they present the interface instability which involves the branching. The lower sedimentary cone consists of the small ceramic inclusions which are enveloped by the austenite. The higher sedimentary cone grows when the broken branches (fragments of oriented dendrites) appear and move towards the ingot axis due to the activities of viscosity gradient together with the gravity. Thus, according to the structures' scheme shown in Fig. 1, both sedimentary cones are the result of the operation of Stokes' law.

* "CELSA – HUTA OSTROWIEC" COMPANY LTD, 27 400 OSTROWIEC ŚWIĘTOKRZYSKI, 2 SAMSONOWICZA STR., POLAND
** INSTITUTE OF METALLURGY AND MATERIALS SCIENCE, POLISH ACADEMY OF SCIENCES, 30 059 KRAKÓW, 25 REYMONTA STR., POLAND
*** ECO-HARPOON – ECOLOGICAL TECHNOLOGIES COMPANY LTD, 05 152 CZOSNÓW, CZĄSTKÓW MAZOWIECKI 152, POLAND

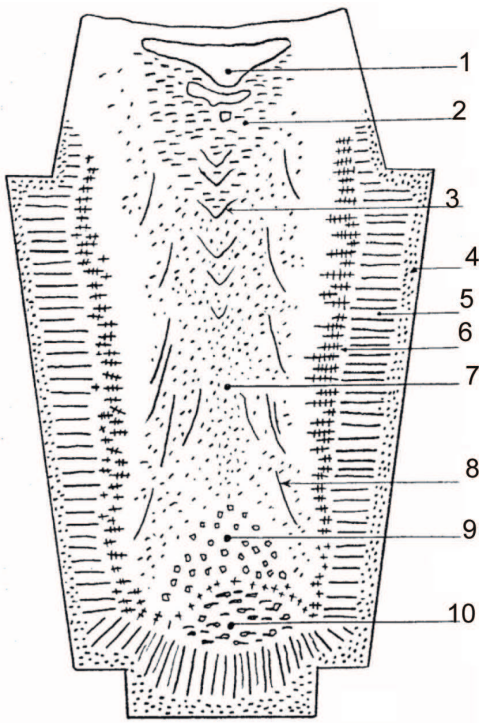

Fig. 1. Structural scheme of the massive forging ingot; 1 – shrinkage cavity, 2 – area with maximum positive segregation, 3 – "V" type segregation, 4 – area with chilled equiaxed grains, 5 – typical columnar structure, 6 – oriented dendrites, 7 – axial porosity with high segregation, 8 – "A" type segregation, 9 – sedimentary cone with the equiaxed grains which manifest negative segregation, 10 – sedimentary cone with contaminated inclusions

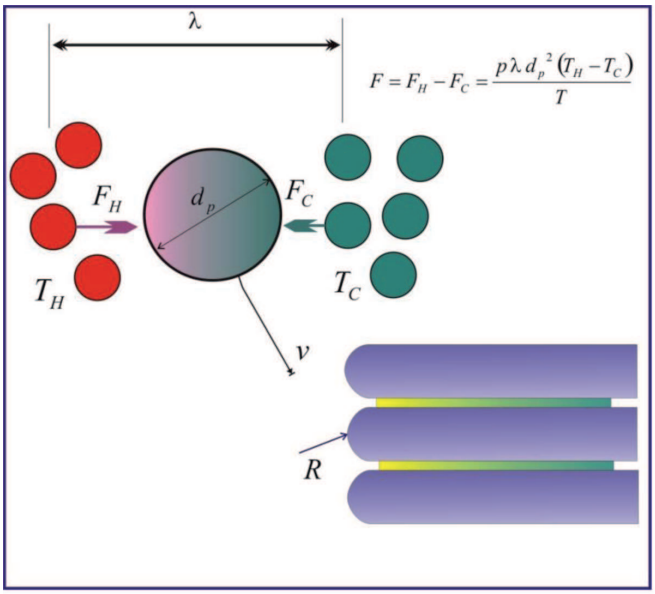

Fig. 2. Principle of the thermophoresis; d_p – diameter of a given equiaxed grain subjected to the gravity; λ – coordination distance between colder liquid atoms (which can be in the direct contact with the analyzed grain) and warmer liquid atoms; T_C – temperature of the colder group of atoms, T_H – temperature of the warmer group of atoms surrounding the analyzed grain; F_C – force of the interplay between colder liquid atoms and analyzed grain; F_H – force of the interplay between warmer group of atoms and analyzed grain; R – radius of the columnar grain tip; v – velocity of the analyzed grain as it results from the activity of gravity force and thermophoresis force; T – analyzed grain temperature; p – static pressure in the liquid which surrounds the analyzed grain.

All the time the thermophoresis phenomenon is in competition with the operation of viscosity gradient. When the formation of the sedimentary cones is completed then the thermophoresis is the winner in the mentioned competition. At that time the formed equiaxed grains are deposited at the surface of the solid due to the dominant activity of thermophoretic force and gravity. The principle of the cooperation between thermophoretic force and gravity force is explained in Fig. 2.

It is evident that columnar grains growth is accompanying by the relatively high thermal gradients observed at the solid / liquid interface, [1]. The equiaxed grains growth requires moderate thermal gradients, [2]. Thus, the transition period of time when the columnar structure transforms into equiaxed structure, involves appearance of the critical thermal gradient which is constant, [3], [4].

Therefore, it can be concluded that the viscosity gradient operates to form an ingot morphology as long as columnar structure, oriented dendrites and both sedimentary cones are formed. When the *liquidus* isotherm makes the liquid undercooled, the thermal gradients observed in the bulk liquid are so small that the thermophoresis dominates exclusively. It is shown schematically in Fig. 2, where the thermophoresis pushes the equiaxed dendrite towards the oriented structure formed formerly during the period of the viscosity gradient's activity. Thus, the thermophoresis is the winner of the discussed competition just at the moment when columnar structure into equiaxed structure transforms, Fig. 3.

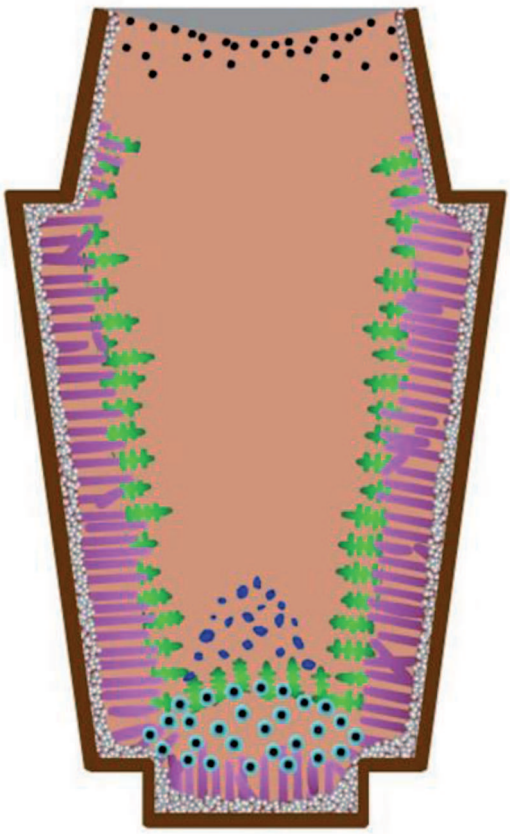

Fig. 3. An ingot morphology at the moment when the activity of viscosity and density gradients is completed; two sedimentary cones are visible in the morphology

Some segregation defects appear during the period of time when the viscosity gradient operates:

a/ significant segregation in the liquid contained in some grooves which exist between the columnar structure; the liquid is enriched in carbon; thus some carbides appear in the grooves, solidification of the remained liquid is accompanied by the appearance of micro-fissures,

b/ significant segregation in the low-melting liquid contained between dendrites' branches; low-melting liquid solidifies within the closed areas which is accompanied by the appearance of the micro-fissures and precipitation of carbides; the existence of the low-melted phases, carbides and micro-fissures within the grooves and inter-dendritic areas can promote the propagation of some cracks during the ingot forging,

c/ the first sedimentary cone contained ceramic particles enveloped by the austenite; ceramic particles should not be present in the ingot's structure,

d/ higher sedimentary cone manifests negative macro-segregation which is not required,

e/ especially danger is the sulphur within the inter-grains regions because it causes the cracks during solidification, Fig. 4.

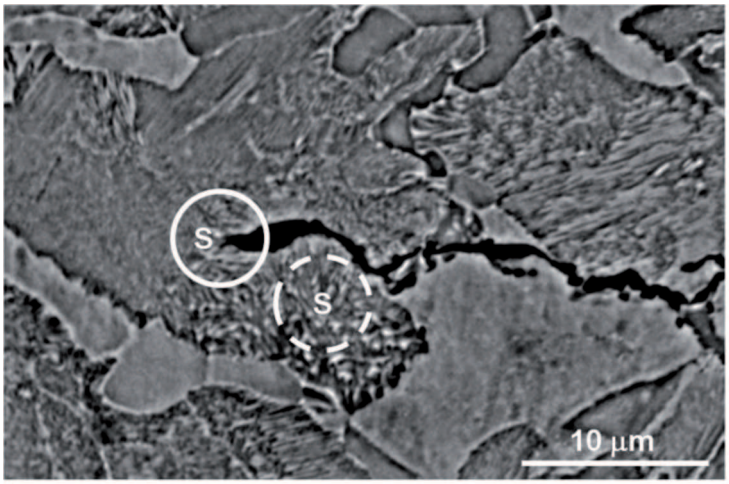

Fig. 4. A crack observed in the forging ingot as the result of increased amount of the sulphur, denoted as the S – areas, [5]

Much significant segregation defects appear during the operations of the thermophoresis. The final morphology of an ingot (after the thermophoresis operations) is shown in Fig. 5.

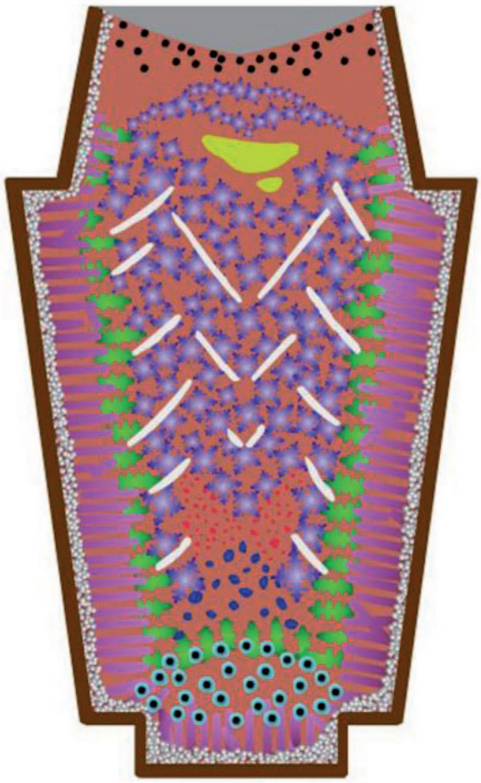

Fig. 5. Final morphology of an forging massive ingot; a "crater" is visible in the ingot morphology; the sedimentary crater is the result of the deposition of some equiaxed grains and first of all is the result of the deposition of some fragments of the equiaxed grains on the sedimentary cone; fragments appear due to some collisions of the equiaxed grains when they form the so-called "dendrites rain"

Some segregation defects which appear during the period of thermophoresis activity are:

a/ canal microsegregation accompanying the deposition of some equiaxed grains on the surface of generating line of the higher sedimentary cone; it yields the appearance of the "A" type macrosegregation,

b/ canal micro-segregation accompanying the deposition of some equiaxed grains on the generating line of the sedimentary crater; it involves the appearance of the "V" type macrosegregation, Fig. 5,

c/ significant microsegregation in the low-melting liquid contained between equiaxed dendrites' branches; low-melting liquid solidifies within the closed areas which is accompanied by the appearance of the micro-fissures and precipitation of carbides; the existence of the low-melted phases, carbides and micro-fissures within the inter-dendritic areas can promote the propagation of some cracks during the ingot's forging,

d/ macro-bands of the big size carbides, they have the same origin as the "A" or "V" - type macrosegregation effects,

e/ significant axial porosity which appears due to the precipitation of low melting phases at the ingot axis; the low melting elements are rejected from the solid / liquid interface and pushed towards the ingot axis; some cracks and empty spaces are formed during their solidification.

The all mentioned segregation defects can promote some cracks in the final product obtained by the forging. However, the lapping of the ingot's defects is also expected. Therefore, few different reforging degrees are applied to the studied ingot to record an annihilation of segregation defects or a formation of the cracks similar to that shown in Fig. 4.

2. Structural observations of the massive forging ingot

The morphology observations performed in a forging ingot produced in the CELSA – Huta Ostrowiec prove that:

a/ columnar grains contain small carbide particles, Fig. 6a; sporadically, some larger precipitates are localized at the columnar grains boundaries, Fig. 6b,

b/ equiaxed grains of the ingot also contain some carbide particles but first of all some bands of carbides of the large size are situated among the equiaxed grains, Fig. 7.

Fig. 6. a. Morphology of the forging ingot (CELSA – Huta Ostrowiec) observed just at the ingot surface; the small carbide particles are localized inside the austenite columnar grains

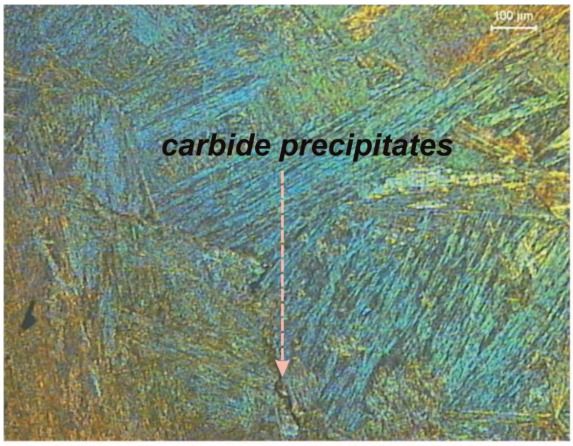

Fig. 6. b. Morphology of the forging ingot (CELSA – Huta Ostrowiec) observed just at the ingot surface; the carbide precipitates are localized at the boundary of the austenite grains

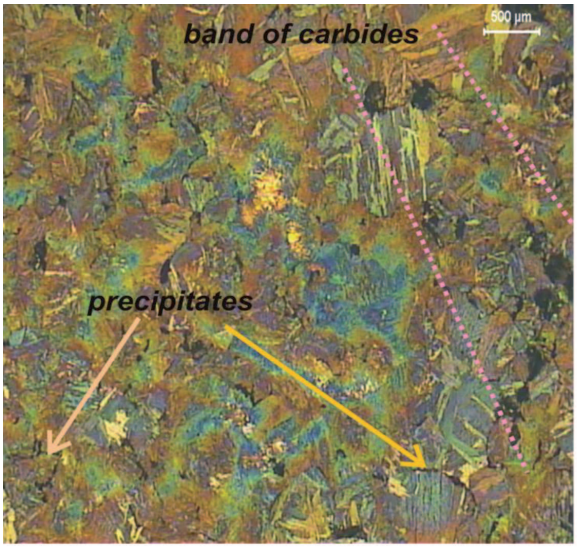

Fig. 7. Morphology of the forging ingot (CELSA – Huta Ostrowiec) observed just at the ingot axis; the carbide precipitates are localized at the boundary of the austenite equiaxed grains; a band of the large size carbides is marked

Some authors consider the rejection / trapping of the particles by the moving solid / liquid interface being in the thermal gradient field, [6]–[11]. According to their considerations a critical velocity of the s/l interface is mainly responsible for the rejection / trapping phenomenon. The morphology observations, Fig. 6. and Fig. 7. prove that the particle radius (size) has also a huge effect on the rejection / trapping phenomenon. Generally, the small size carbides were trapped by the austenite grains, Fig. 6a, while the bigger carbides were rejected to the boundaries as the precipitates, Fig. 6b., Fig. 7.

The very large carbides form the bands, Fig. 7. The discussed phenomenon of the carbides formation leads to the appearance of some areas within which the carbon macrosegregation is positive or negative, Fig. 8.

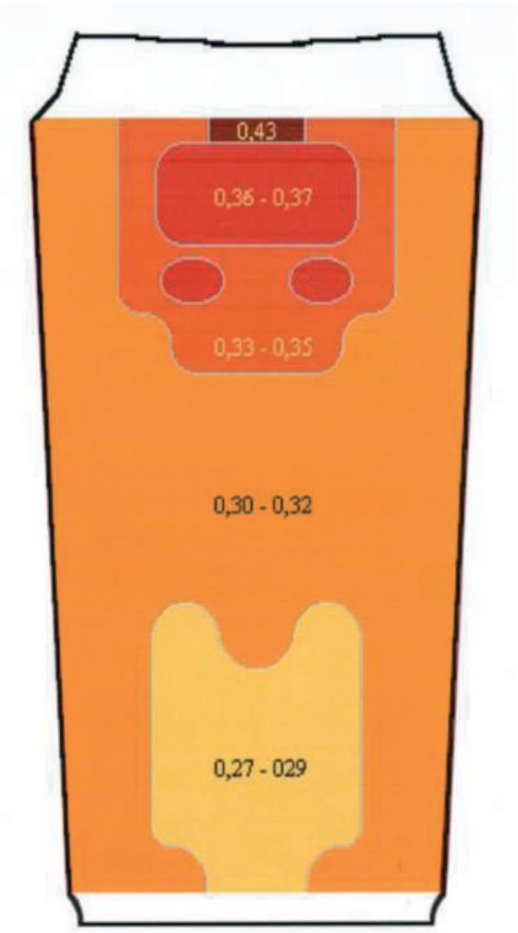

Fig. 8. A macrosegregation map of the carbon at the mean longitudinal section of the middle-massive ingot with nominal concentration of carbon: 0.32%; negative macrosegregation is visible at the ingot bottom; almost nominal carbon concentration is observed in the middle of ingot; three areas with the different positive carbon macrosegregation are revealed in the upper part of the ingot

A macrosegregation map of the carbon developed for the massive forging ingot, Fig. 8 can be subjected to the confrontation with the localization of different structural areas shown in Fig. 1 or Fig. 5. First of all, the areas containing 0.30-0.32%C, Fig. 8 correspond well with the areas within which the columnar structure was formed, Fig. 1, Fig. 3. The areas with negative carbon macrosegregation, (ingot's bottom, Fig. 8) can be referred to the formation of both sedimentary cones. In fact, low carbon austenite grains are formed within the cones.

The almost nominal carbon concentration is observed above the sedimentary cones. The equiaxed austenite grains appear in this area. They are growing very slowly from the undercooled liquid so that the back-diffusion parameter is close to unity for this growth. Subsequently, the equiaxed grains contain almost nominal carbon concentration and precipitates are not large.

Next solidification accelerates and the appeared equiaxed grains are localized on the slope of the third cones which can be distinguished within the ingot morphology, Fig. 9.

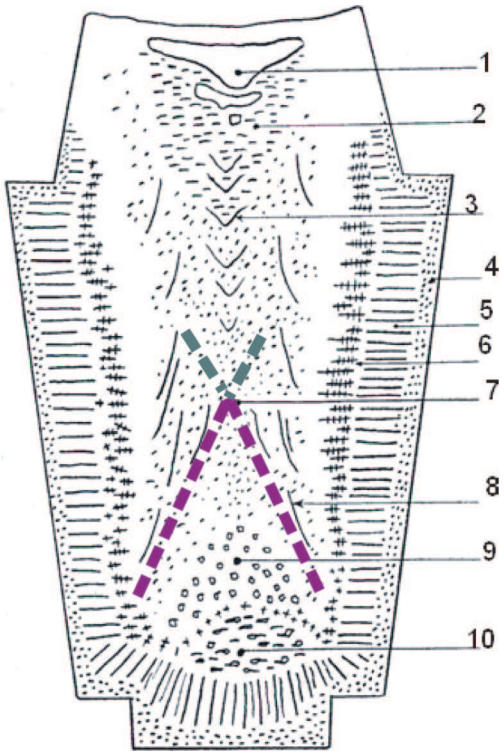

Fig. 9. A hypothetical localizations of: a/ a third sedimentary cone (red dashed line) and b/ a crater which promotes the formation of the "V" – type macrosegregation (green dashed line)

Since the grains are formed more rapidly the amount of precipitates increases. The precipitates are now subjected to canal microsegregation and form as if a wave of precipitate bands visible as the "A" type macrosegregation. There are a lot of sulphur and low melting phases. The macrosegregation map, Fig. 8, does not reveal the „A" – type macrosegregation. This is justified because the macrosegregation map presents an average concentration of carbon within a given ingot's region.

The similar phenomenon of canal microsegregation is observed in the upper part of ingot where the "V" type macrosegregation appears. The equiaxed grains are localized on the slope of the crater which is formed within this region, Fig. 9. The "V" type macrosegregation is the result of the canal microsegregation which forms as if a wave of precipitate bands. In this area not only axial porosity appears but the positive macrosegregation of the carbon is observed. The positive carbon macrosegregation appears because the carbon rejected from the solid / liquid interface of columnar grains, oriented dendrites and equiaxed dendrites is pushed towards the ingot's axis and then towards the upper part of the ingot. It is recorded in Fig. 9.

3. Acoustic identification of the defects within the massive forging ingot

The morphology of an ingot is usually observed by the Light Microscopy. However, the Light Microscopy is not able to reveal all the details of morphology of some single defects as these shown in Fig. 10. Therefore, an attempt to identify the details of some defects was done by the Scanning Acoustic Microscopy, Fig. 11, Fig. 12, Fig. 13.

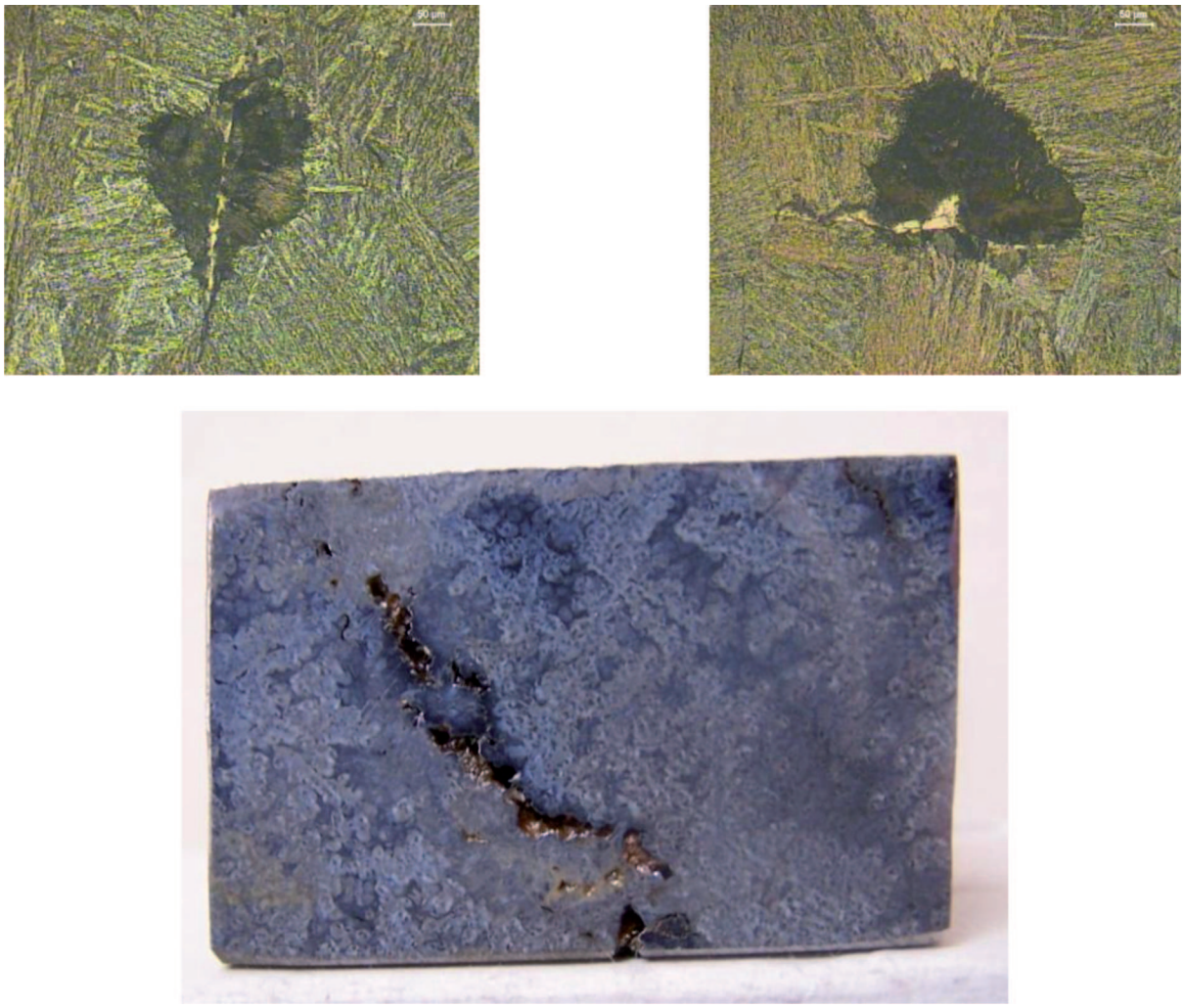

Fig. 10. Typical defects revealed in the forging ingot by the Light Microscopy; a/ b/ inclusion surrounded by the carbide, c/ precipitate of the sulphur and low melting phases, [5]

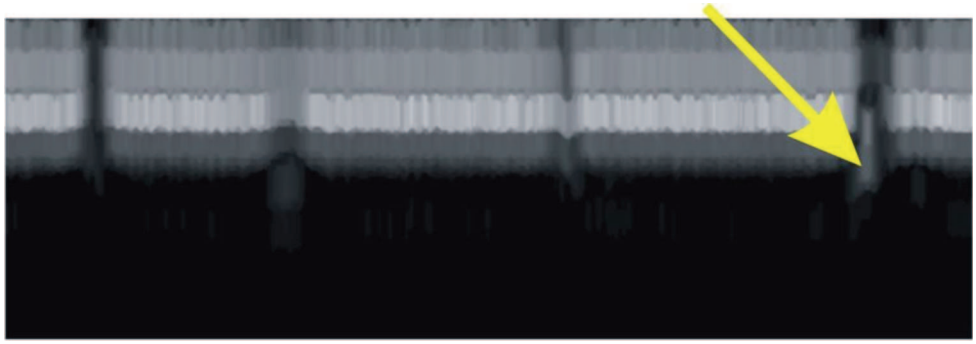

Fig. 11. Scanning Acoustic Microscopy identification of defects at different depths from the surface; observation made within the subsequently localized sub-layers. Four defects (holes) are visible; fourth defect contains a carbon stalagmite (yellow arrow indicates the carbide localized inside the void)

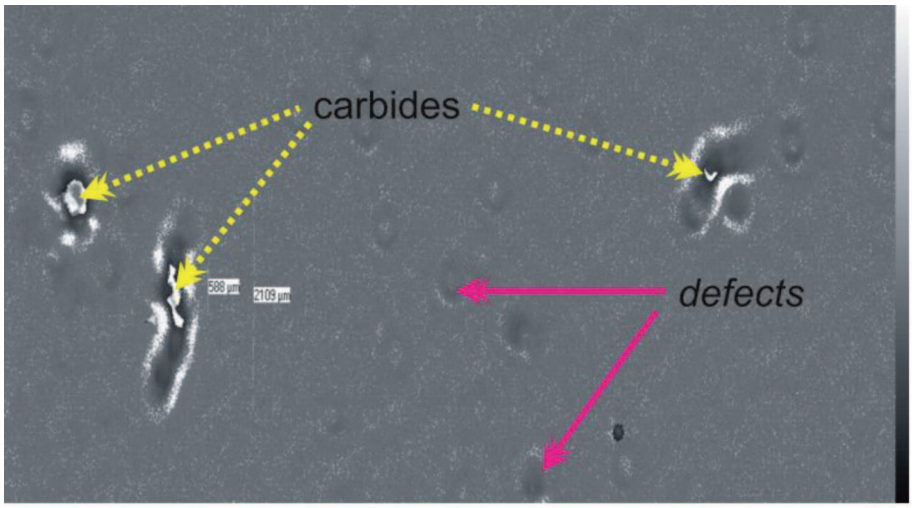

Fig. 12. Top view of the observation area; the Scanning Acoustic Microscopy allows to distinguish carbides localized inside the void and common defects (porosity)

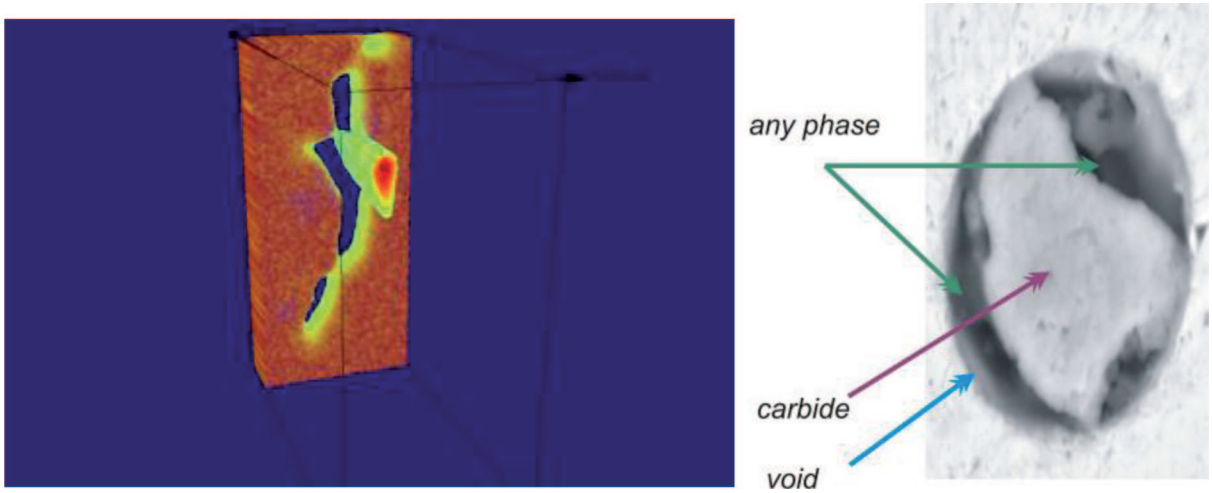

Fig. 13. Confrontation of the computer 3D visualization of a defect observed by the Scanning Acoustic Microscopy with the real defect revealed by the microscope; a/ a carbide stalagmite situated in the void, b/ cross-section of a carbide surrounded by any phase and a void

4. Geometry of the forging ingot and geometry of reforged ingot

The selected forging ingots have been cut into slices as marked in Fig. 14.

Next, the ingot was subjected to the preliminary plastic deformation (forging) to obtain a roll – like ingot of the diameter equal to 850 mm. Finally, the roll – like ingot was subjected to final plastic deformation with different reforging degrees, Fig. 15.

Some slices were obtained due to the performed cutting of the reforged ingot, Fig. 16.

The samples for analysis were taken from each slice. Localization of the samples is shown in Fig. 17.

According to the geometry shown in Fig. 15 some different reforging degrees were imposed to the ingot, Table 1.

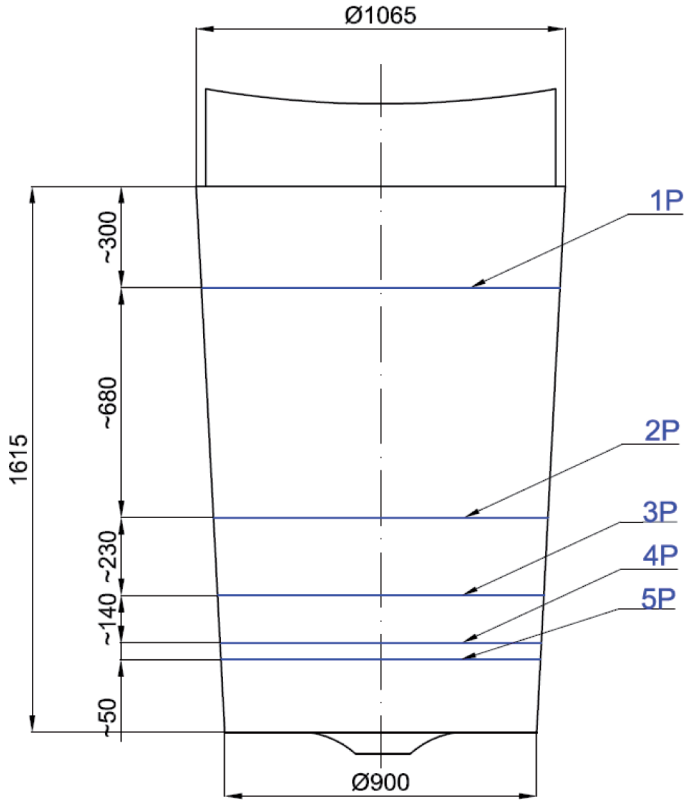

Fig. 14. Geometry of the forging ingot selected to the analysis; five cross-sections (1P-5P) are marked due to the predicted cutting

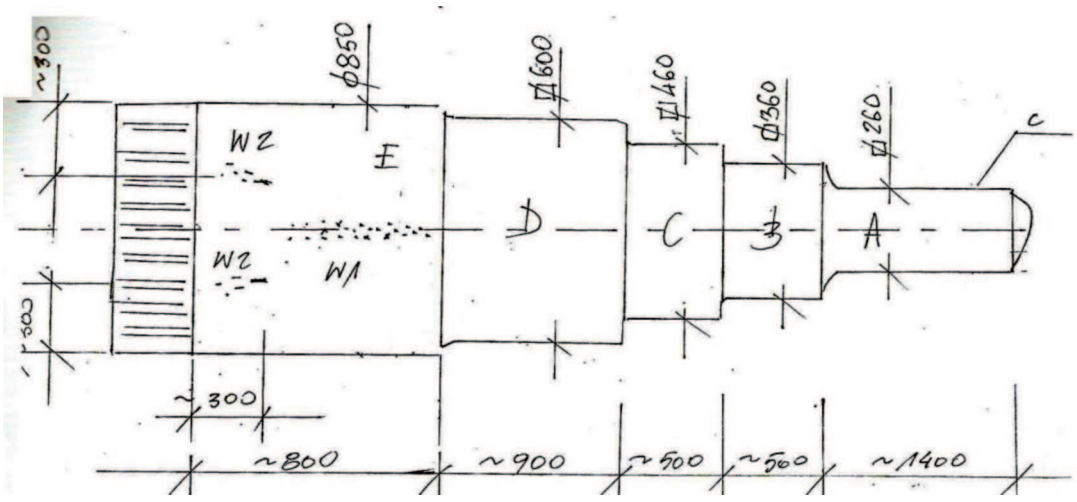

Fig. 15. Geometry of the ingot subjected to the plastic deformation. Axial porosity and porosity referred to the shrinkage cavity are marked in the E – region of the reforged ingot

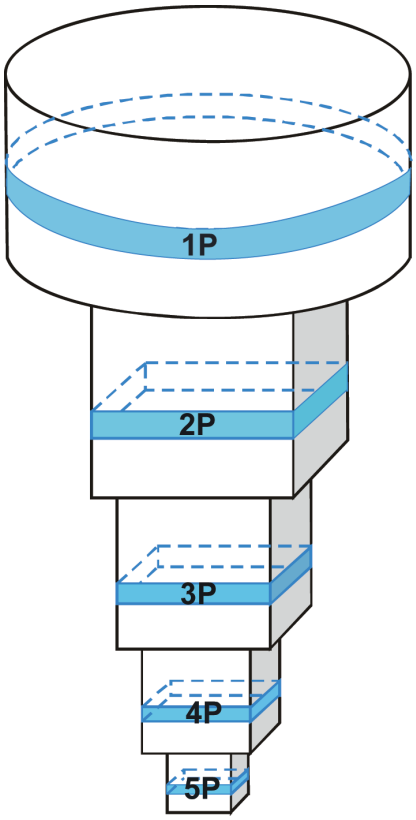

Fig. 16. Localization of the slices within the reforged ingot

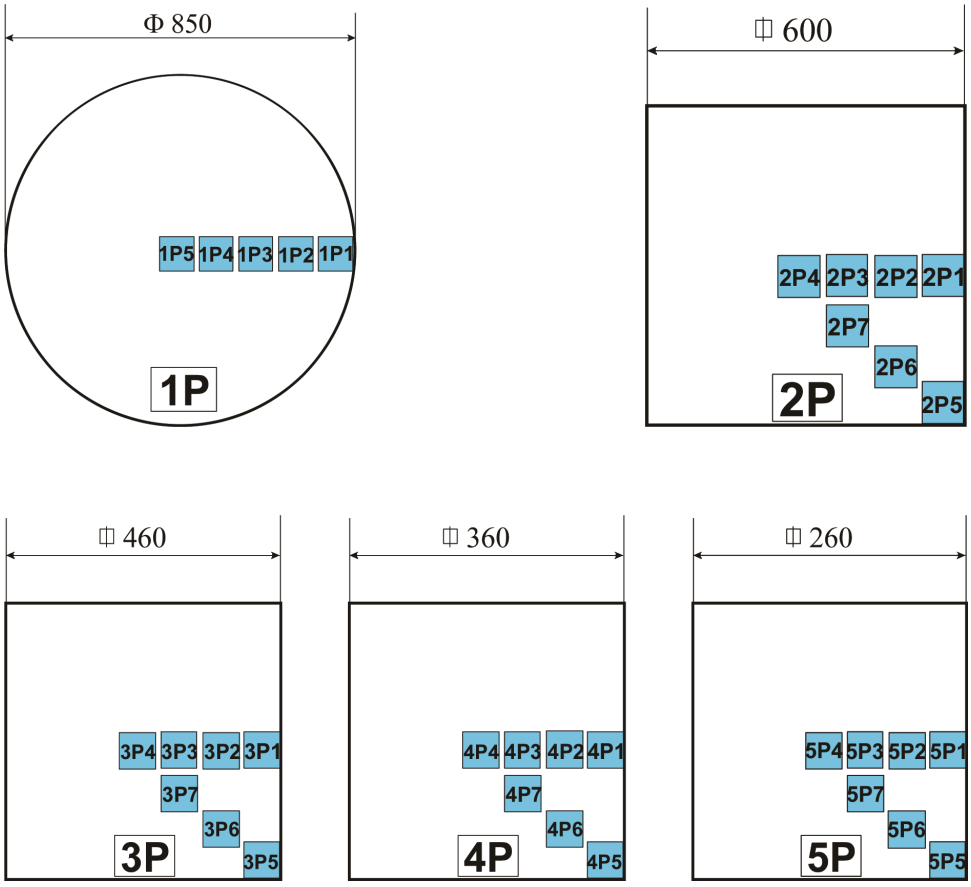

Fig. 17. Localization of the samples on the surface of different slices taken from the forged ingot shown in Fig. 16

TABLE 1

Reforging degrees applied to the analyzed forging ingot

mark of the ingot segment	denotation of the slice	reforging degree, r_i
E	1P	1.00
D	2P	1.58
C	3P	2.68
B	4P	4.38
A	5P	8.39

The two-dimensional reforging degree, Table 1, is defined as follows:

$$r_i = A_1/A_i, \quad i = 1, ..., 5 \tag{1}$$

A_i – cross-section surface of the reforged ingot segments, (E, D, C, B, A), Fig. 15.

The reforging was carried out for the ingot heated till 1220°C. The ingot temperature decreases to 880°C during the analyzed process, Fig. 18.

5. Density measurement within the reforged ingot

Since the intensity of the defects distribution depends on the analyzed reforged ingot region it is justified to measure the density in its different segments. The systematic error of the density measurement was about 0.03%. The results of the density measurement are gathered in Table 2.

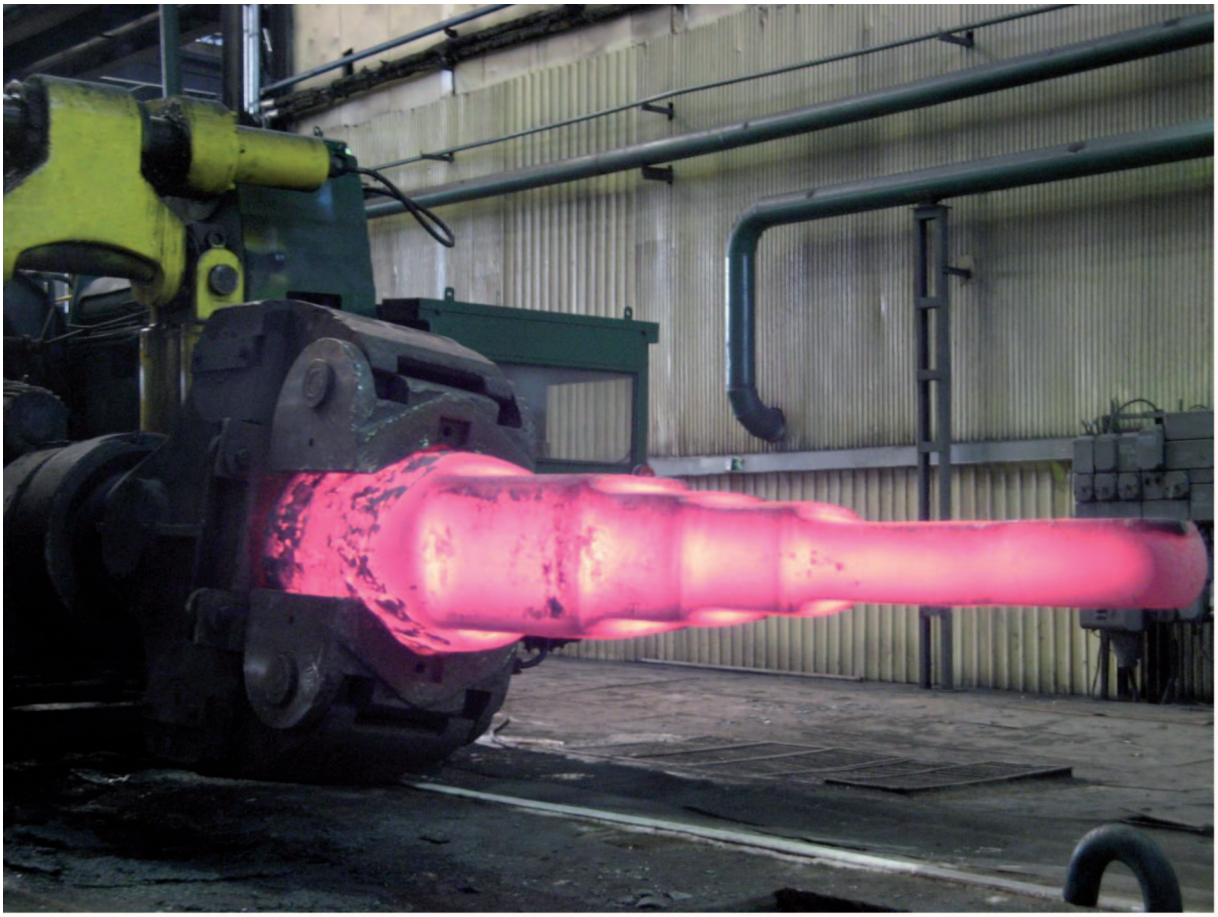

Fig. 18. Transportation of the reforged ingot (CELSA – Huta Ostrowiec)

TABLE 2

Density of the reforged ingot

density, ρ	slice number				
sample number	1P	2P	3P	4P	5P
1	7.8540	7.8540	7.8586	7.8576	7.8576
2	7.8570	7.8575	7.8574	7.8548	7.8570
3	7.8530	7.8570	7.8596	7.8587	7.8558
4	7.8490	7.8560	7.8596	7.8582	7.8601
5	7.6130	7.8550	7.8555	7.8572	7.8593
6		7.8550	7.8570	7.8560	7.8560
7		7.8550	7.8578	7.8602	7.8583

The results of the density measurement are also presented in Figs 19.-23.

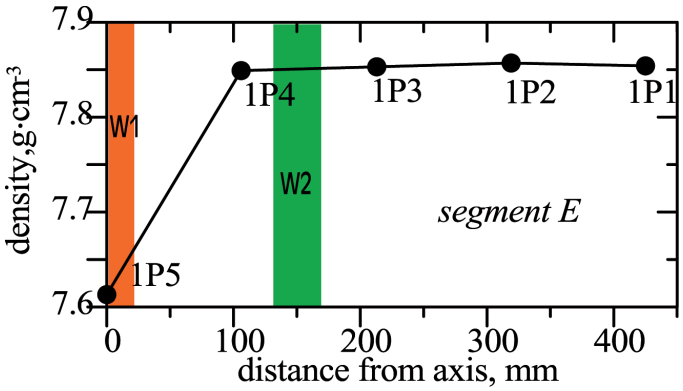

Fig. 19. Density of the E – ingot segment reforged preliminary from ϕ 1065 (Fig. 14) to ϕ 850 (Fig. 15) with the reforging degree equal to ~1.3

The smallest density is observed for the sample 1P5, Fig. 19. It is connected with the W_1 – axial porosity which is marked within the E – segment, Fig. 15. It seems that the preliminary reforging applied to the E – segment was sufficient to obtain satisfactory consolidation of the ingot (W2 – area shown in Fig. 19). The maximum consolidation was obtained in the case of the 1P4 – sample, Fig. 19.

It is evident that the axial part of the ingot (the E – segment) requires radical consolidation. The following consolidation factor can be defined for each of envisaged ingot segment:

$$w_i = [1 - \rho_{\min}^{segment}/\rho_{\max}^{segment}]\ 1000 \quad i = E, D, C, B, A \quad (2)$$

The values of the consolidation factor are gathered in the Table 3. The higher is the value of the w_i – factor the more intensive consolidation is required for a given ingot segment.

TABLE 3

Local consolidation factor as calculated for the analyzed reforged ingot segments

mark of the ingot segment	consolidation factor [$^0/_{00}$]	reforging degree
E	w_E = 31.055	1.00
D	w_D = 0.445	1.58
C	w_C = 0.522	2.68
B	w_B = 0.687	4.38
A	w_A = 0.547	8.39

The value of the w_E factor is elevated, Table 3, because the W_1 – axial porosity is not overlapped within the E – segment. The W_2 co-axial porosity seems to be partially overlapped. The week consolidation results from the fact that the preliminary reforging was applied to the E – segment, only. Preliminary reforging degree applied to the E – segment equals ~1.3.

The value of w_D and w_C – factors is small and it would suggest that the steel is almost perfectly consolidated within this area, Table 3. However, this is misleading conclusion because the maximum density within the D and C – segments is also small. The maximum density is small because the porosity is elevated in these both segments and was not perfectly overlapped. Also, some voids are not yet recovered in these segments. Moreover, the "V" type and "A" type macrosegregation defects are localized there.

Therefore, the total consolidation factor w_i^{total} is to be analyzed, Table 4.

The total maximum value of the density $\rho_{\max}^{total}$ is equal to 7.8602, Table 2. Therefore, the total consolidation factor is defined as follows:

$$w_i^{total} = [1 - \rho_{\min}^{segment}/\rho_{\max}^{total}]\ 1000 \quad i = E, D, C, B, A \quad (3)$$

Table 4 contains the values of the total consolidation factor. It informs about the potential w_i^{total} theoretically possible consolidation for a given ingot segment.

TABLE 4
Total consolidation factor as calculated for the analyzed reforged ingot segments

mark of the ingot segment	consolidation factor [$^0/_{00}$]	reforging degree
E	w_E^{total} = 31.450	1.00
D	w_D^{total} = 0.789	1.58
C	w_C^{total} = 0.662	2.68
B	w_B^{total} = 0.687	4.38
A	w_A^{total} = 0.560	8.39

The value of the w_B – factor is higher than the value of the w_C – factor. Also, the value of the w_B^{total} factor is higher than the value of the w_C^{total} – factor. It results from the fact that the major part of the lower sedimentary cone with contaminated inclusions (Fig. 1) is located there.

The value of the w_A – factor value is lower than the value of the w_B factor, Table 3. Also, the value of the w_A^{total} factor is lower than the value of the w_B^{total} – factor, Table 4. It results from the fact that this ingot part manifest a negative macrosegregation of carbon, Fig. 8. Additionally, the A – ingot segment was subjected to the higher plastic deformation, Table 1.

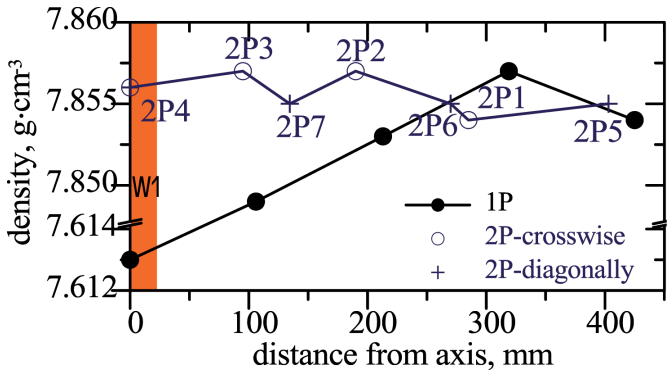

Fig. 20. Density of the D – segment of the reforged ingot

The density of the sample 2P4 can be compared with the density of the sample 1P5, Fig. 20. At the reforging degree applied to the D – segment, the axial porosity was overlapped to a considerable extent (for the distance from ingot axis equal to zero, Fig. 20).

However, the decrease of density is visible while comparing the density of the sample 2P6, 2P1 and 2P5 with the density of sample 1P4. It is suggested that the discussed decrease of the density is the result of the presence of the "A" type macrosegregation effect shown schematically in Fig. 5.

Generally, the ingot consolidation is substantial within the D – segment, especially within the 0 to 250 mm range of the ingot radius, Fig. 20.

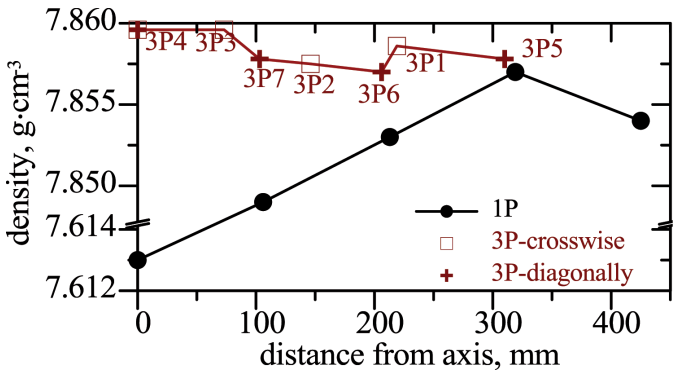

Fig. 21. Density of the C – segment of the reforged ingot

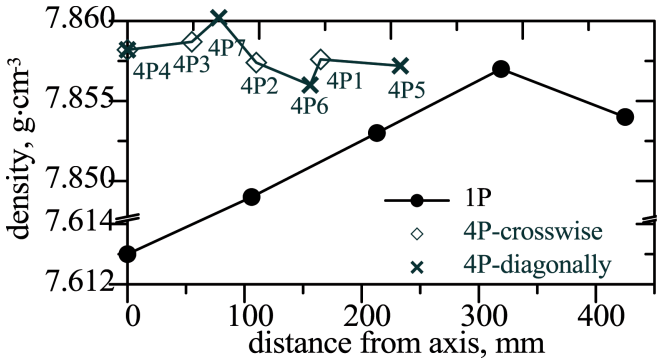

Fig. 22. Density of the B – ingot segment of the reforged ingot

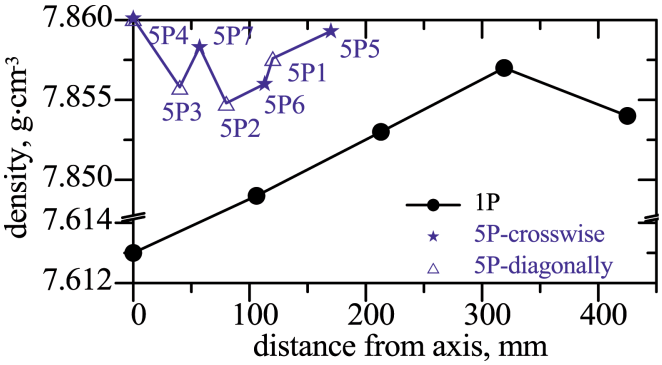

Fig. 23. Density of the A – ingot segment of the reforged ingot

The ingot consolidation resulting from the plastic deformation can also be observed along the reforged ingot, Fig. 24.

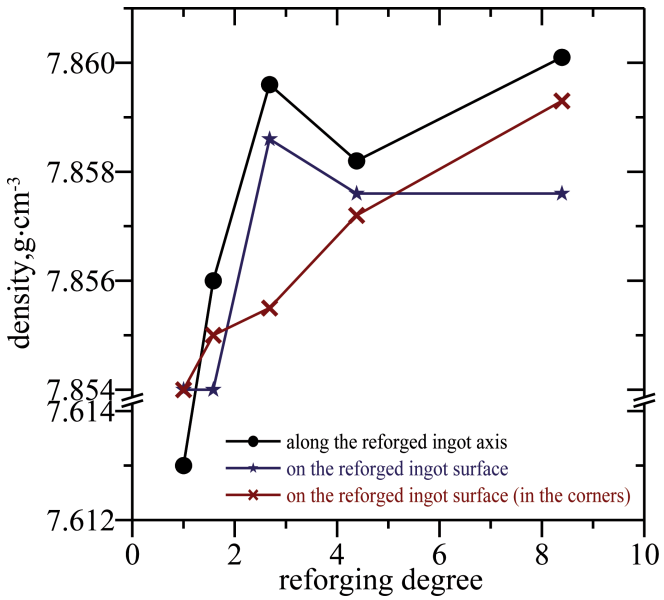

Fig. 24. Density observed along the analyzed reforged ingot

The density behavior can be studied along the reforged ingot but comparison is made between maximum density / average density / minimum density for each segment, Fig. 25. The curves are drawn due to the results gathered in Table 2.

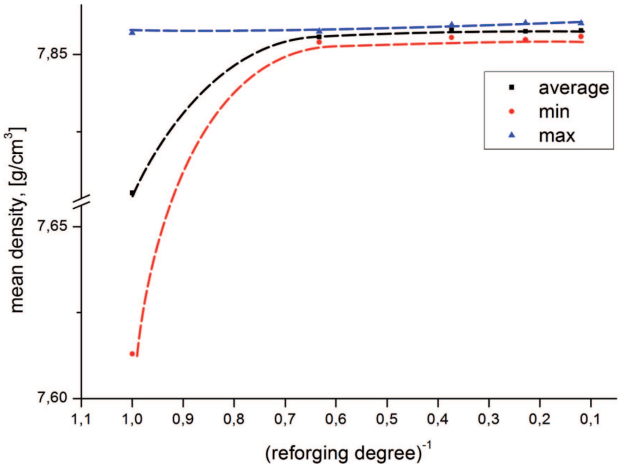

Fig. 25. Comparison of the local densities after applied reforging degree

6. Acoustic identification of the defects in the reforged ingot

The plastic deformation applied to the forging ingot should ensure partial or even complete overlapping (closure) of the voids, cracks and faults. Some investigations of the problem are known in the bibliography, [12] – [14]. Also, the second phase particles (carbides) have a significant influence on the microstructure evolution [15]. According to the mentioned studies the closure of the faults is possible to some extent. In spite of this, Wang and Zhong [12] suggest to carry the cast processes under vacuum in order to avoid the formation of some voids.

The systematic observation of the ingot defects was not made in the current work. Some defects found by chance have been only studied, Fig. 10. – Fig. 13. Therefore, the comparison of cracks, voids, faults and fissures before reforging and just after it cannot be made efficiently. In spite of this fact, the samples: 1P5, 5P2 and 5P4 were subjected to the ultrasonic inspection. This inspection allows to identify the defects, which were not overlapped (closed) by the applied plastic deformation. An example of observation is shown in Fig. 26.

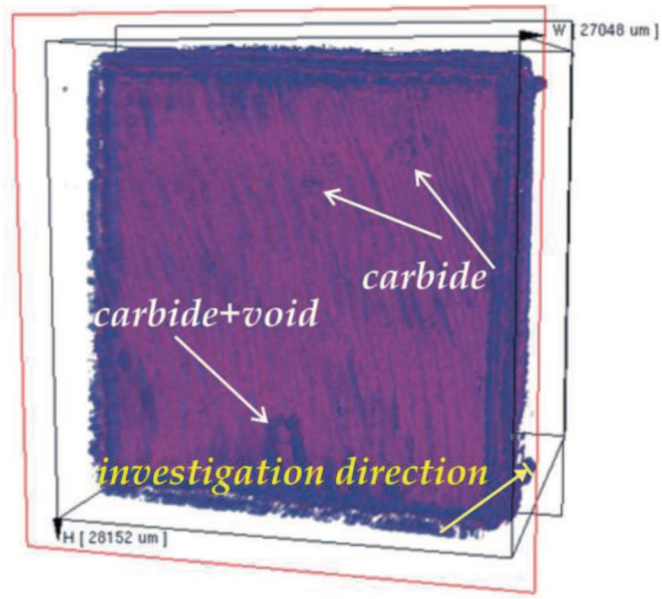

Fig. 26. Ultrasonic inspection of the sample 1P5 applying the method: "layer by layer" from its surface towards the interior

The performed ultrasonic inspection proves that the cracks and void were generally overlapped (closed) by the plastic deformation. Practically, some carbides are visible within the studied sample, as shown in Fig. 26 for the first studied layer situated just at the sample surface.

7. Concluding remarks

- the existence of the third sedimentary cone is suggested; the formation of this cone should, however, be confirmed by the proper numerical simulation of the heat transfer in the forging massive ingot; it is supposed that the third sedimentary cone, Fig. 9, is the result of common activities of the Stokes' law, Magnus force, gravity and phenomenon of thermophoresis, all supported by the convection;
- the third cone should contain the equiaxed grains, only; it is justified since the "A" - type macroseg-

regation (which follows the cone formation) appears within the zone of equiaxed grains,

- some measurements of the density in the ingot before deformation, manifest twice the decrease of this parameter in the regions of: a/ equiaxed structure, b/ axial region, Fig. 27; it corresponds well to the observations of porosity in the E – zone, Fig. 15,

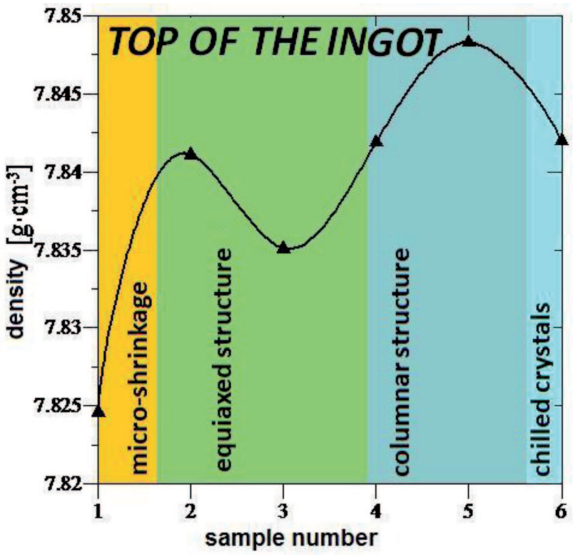

Fig. 27. Density of the ingot's E-zone as observed before the reforging

- some observations of the forging ingot confirm the presence of the cracks, voids and porosity, Fig. 4, Fig. 6, Fig. 10, Fig. 11, Fig. 12, Fig. 13; even small plastic deformation leads to radical steel consolidation, Fig. 28,
- it seems that the consolidation was not so effective in the neighborhood of the point 4P, Fig. 28, where the sedimentary cone with the contamined inclusions can be localized,
- the redistribution of carbon in the macro-segregation map, Fig. 8, obtained experimentally corresponds well with the presented structural scheme of the forging ingot, Fig. 1, Fig. 3,
- a new consolidation factor can also be defined as a ratio of the maximal density within a given ingot segment (A, B, C, D, E) and the maximal density found in the whole ingot.

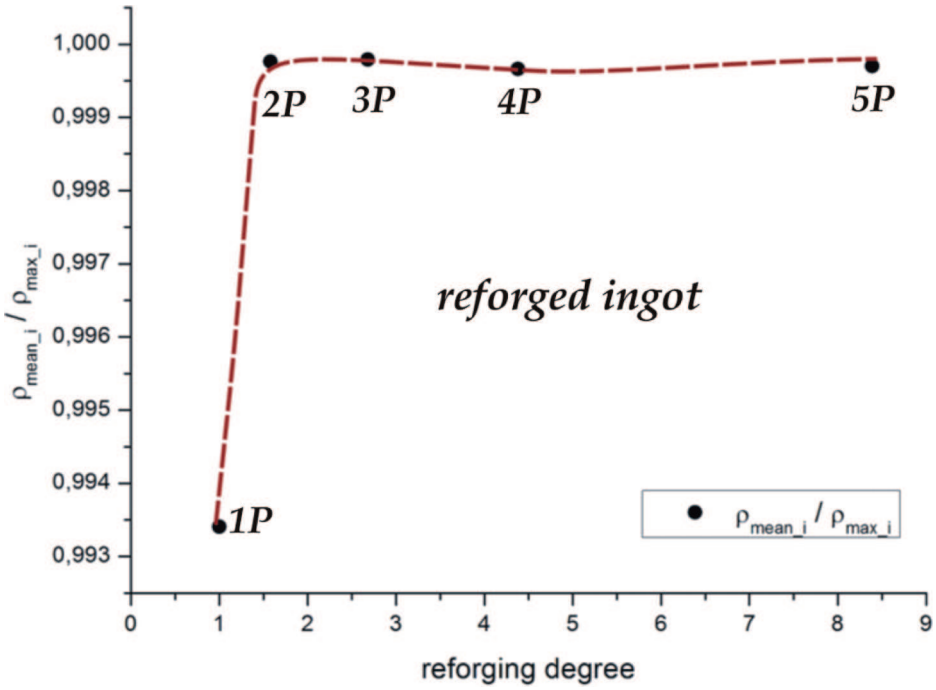

Fig. 28. Normalized density of the ingot in function of the reforging degree

Acknowledgements

The financial support from the Polish Ministry of Science and Higher Education (MNiSW – Poland) under the contract: N R15 006 004 is gratefully acknowledged.
The assistance of the "Huta Buczek; Sosnowiec, Poland" and the "CELSA – Huta Ostrowiec; Ostrowiec Św., Poland" is greatly appreciated.

REFERENCES

[1] J.D. Hunt, Steady State Columnar and Equiaxed Growth of Dendrites and Eutectics, Materials Science & Engineering **65**, 75-83 (1984).
[2] W.S. Wołczyński, Constrained/Unconstrained Solidification within the Massive Cast Steel/Iron Ingots, Archives of Foundry Engineering **10**, 195-202 (2010).
[3] W.S. Wołczyński, E. Guzik, W. Wajda, B. Kania, Columnar ==> Equiaxed Structure Transition in Solidifying Rolls, Proceedings of the 14 International Heat Transfer Conference, Washington – 2009, Melting and Solidification, IHTC14-23048, 9.1-9.10.
[4] W.S. Wołczyński, B. Kania, W. Wajda, M. Kostrzewa, Space – Time – Structure Map for As Cast Massive Rolls, Proceedings of the ASME/JSME 2011 8th Thermal Engineering Joint Conference AJTEC2011, Honolulu – Waikiki – 2011, Fundamental of Heat and Mass Transfer; Computational Heat and mass Transfer, AJTEC2011-44021, p. 3.1-3.9.
[5] J. Kowalski, J. Deda, A.M. Janus, R. Martynowski, W.S. Wołczyński, Ultrasonic Method Applied to Defects Identification in the Forging Ingots, Inżynieria Materiałowa **175**, 260-263 (2010).
[6] P. Hoekstra, R.D. Miller, On the Mobility of Water Molecules in the Transition Layer between Ice and a Solid Surface, Journal of Colloid Interface Science **25**, 166-173 (1967).
[7] R.R. Gilpin, Model for the "Liquid-Like" Layer between Ice and a Substrate with Applications to Wire Regulation and Particle Migration, Journal of Colloid Interface Science **68**, 235-251 (1979).
[8] J.K. Kim, P.K. Rohatgi, An Analytical Solution of the Critical Interface Velocity for the Encapturing of Insoluble Particles by a Moving Solid / Liquid Interface Metallurgical and Materials Transactions **29A**, 351-358 (1998).
[9] J.K. Kim, P.K. Rohatgi, The Effect of the Diffusion of Solute between the Particle and the Interface on the Particle Pushing Phenomena, Acta Metallurgica **46**, 1115-1123 (1988).
[10] J.K. Kim, P.K. Rohatgi, Interaction between Moving Cellular Solidification Front and Graphite Particles During Centrifugal Casting, Materials Science and Engineering **244A**, 168-177 (1998).
[11] R. Sasikumar, T.R. Ramamohan, B.C. Pai, Critical Velocities for Particle Pushing by Moving Solidification Front, Acta Metallurgica **37**, 2085-2091 (1989).
[12] Q. Ma, Z. Wang, Y. Zhong, The Mechanism of Faults Originating from Inclusions in the Plastic Deformation Processes of Heavy Forging, Journal of Materials Processing Technology **123**, 61-66 (2002).
[13] C.Y. Park, D.Y. Yang, Modeling of Void Crushing for Large-Ingot Hot Forging, Journal of Materials Processing Technology **67**, 195-200 (1997).
[14] X.X. Zhang, Z.S. Cui, Theoretical Study of Void Closure in Nonlinear Plastic Materials, Applied Mathematics and Mechanics **30**, 631-642 (2009).
[15] H. Paul, T. Baudin, F. Brisset, The Effect of the Strain Path and the Second Phase Particles on the Microstructure and the Texture Evolution of the AA3104 Alloy Processed by ECAP, Archives of Metallurgy and Materials **56**, 245-261 (2011).

Received: 10 April 2011.